Journal of Hazardous Materials, 9 (1984) 265—290
Elsevier Science Publishers B V , Amsterdam — Printed in The Netherlands

NUMERICAL INVESTIGATIONS OF NONIDEAL EXPLOSIONS

M S RAJU* and R A STREHLOW

Department of Aeronautical and Astronautical Engineering, University of Illinois, Urbana, IL 61801 (U S A)

(Received January 30, 1984, accepted in revised form April 7, 1984)

Summary

This study focusses on nonideal free field blast waves arising from the finite rate of energy addition in a distributed nonspherical source region The behavior of the blast wave is determined in a compressible medium surrounding a centrally ignited flammable mixture during and after the propagation of a heat addition wave which models the detonative or deflagrative combustion process Numerical integration of the nonsteady, two-dimensional Euler equations is performed by incorporating a heat addition "two-gamma ' working fluid model to represent the flame or detonation wave This study also investigated the behavior of a blast wave generated by the burst of a high-pressure ellipsoid The effect of the heat addition waves on the near and far field blast waves was studied by determining the relevant blast parameters, peak overpressure, and positive phase impulse, as well as the detailed evolution of the gas dynamic variables with time and distance The blast parameters which correspond to low velocity flames compare favorably with those obtained using linear acoustic monopole theory The results indicate that pressure relief associated with the presence of a compressible inert medium surrounding the combustion products after the flame propagates to the interface of nonspherical clouds severely re stricts the intensity of the explosion and thereby reduces the damages that can be produced by the blast wave

I Introduction

The ability of flames to generate damaging blast waves is of interest in connection with the occurrence of a large cloud of a hydrocarbon—air mixture in the atmosphere due to a spill of a high-vapor-pressure or liquid hydrocarbon in the open during manufacture, transport or storage The possibility of such explosions must be considered in assessing the safety of neighboring installations Literature abounds with theoretical studies on spherically symmetric blast waves generated by spherical source regions [1—3] However, in accidental vapor cloud explosions spherical symmetry of the source region is an exception rather than the rule Most accidental explosions are likely to involve heavier-than-air gas clouds either because of the

*Present address University of Dayton, Research Institute, KL-461, Dayton, OH 45469, U S A

0304 3894/84/$03 00

intrinsic density of the fuel in question or because of the low temperature at which it is stored Density and wind effects play a crucial role in the spread and drift of the gas and produce extended, pancake-shaped and/or elongated clouds [4] The study of wave symmetry is an important aspect because the damage pattern from most accidental explosions indicates a high degree of directionality In general, the blast wave generated in accidental explosions is of moderate strength and the degree of wave asymmetry is quite large [5]

Chiu et al [5] presented the solution to the asymmetric blast waves involving the burst of a pressurized ellipsoid based on the Whitham's ray-shock theory and the Brinkley—Kirkwood theory of shock propagation Such an approach has not as yet been extended to an understanding of the blast waves generated by flame propagation Most of the existing studies on asymmetric blast waves generated by deflagrative combustion processes are based on acoustic theory [6, 7] The acoustic theory is only valid for the limiting solution of weak deflagrative explosions For usual hydrocarbon—air mixtures, with the remote exception of powerful direct initiation, immediate detonation is unlikely but not completely excluded as evidenced by a number of forthcoming studies on the detonability of unconfined hydrocarbon—air mixtures Sickel and Foster [8] studied the ground impulse generated by a plane fuel—air detonation with a side relief based on an iterative procedure involving appropriate gas-dynamic relationships Williams [9] presented a qualitative analysis for determining the pressure development subsequent to the ignition of the pancake-shaped clouds in terms of an expansion involving small Mach numbers for flame speed to describe nonlinear wave propagation Such approaches may provide values for pressures which are within the correct order of magnitude but fail to provide a detailed account of the blast behavior and relevant time histories of the location of the shock and the distortion of the cloud with time, which are important to the understanding of directional effects induced by wave asymmetry

The aim of the present investigation is to extend the study of blast waves to one more dimension to include the effects of wave asymmetry generated by three distinct sources of nonideal behavior, i e , those involving the bursting of a high-pressure vessel, and deflagrative and detonative combustion processes Numerical integration of the 2-D nonsteady flows has been carried out with the help of a 2-D hydrocode based on the scheme proposed by Godunov et al [10] To facilitate the numerical treatment of the combustion process the flame is replaced by a "two-gamma" working fluid model developed by Strehlow et al [11], who have shown that a generalized heat addition Hugoniot accurately models steady hydrocarbon—air combustion processes over the range of interest for vapor-cloud explosions The numerical calculations are carried out for some time period after the flame has been extinguished and yield blast parameters out to considerable distances from the source region

II. Governing equations

In this study we are primarily interested in the flowfield generated by a centrally ignited moving flame front in clouds of flammable vapor which have axisymmetric configurations The resulting blast wave creates a nonsteady axisymmetric flowfield in a compressible medium bounded by a gas dynamic discontinuity The products of explosion are separated from the burnt gases by a moving surface which can be either a flame front or a contact discontinuity or a combination of both It is required to calculate the motion of the shock wave, the moving surface separating the burnt and unburnt gases, and the whole flowfield behind the lead shock wave The formulation is idealized in that both the surrounding medium and the products of explosion are considered to be perfect gases with different specific heat ratios, γ_1 and γ_2 The initial combustible region and the undisturbed medium surrounding the shock front are considered to be at rest and homogeneous with pressure $p = p_0$ and density $\rho = \rho_0$

When ignition occurs at the center of an axisymmetric cloud, a spherical flame propagates through the cloud until it breaks through the outer surfaces of the cloud The subsequent shape of the flame depends on the degree of axisymmetry, the type of the cloud, and the flame speed Considering the process of ignition and initial flame acceleration to be out of the scope of this paper, it is assumed that the system has a self-similar flowfield after the completion of the initial spherical flame propagation Following this initial phase of spherical combustion the normal burning speed of the flame, S_u, is assumed to remain constant Such an assumption does not consider the dependence of the flame speed on pressure, temperature, composition of the fuel—air mixture, and the degree of turbulence In this respect the blast wave—flame physics is never addressed in this study

The basic nonsteady, 2-D conservation equations of fluid mechanics in Eulerian form, excluding the energy source terms, the effects of mass injection and body forces (buoyancy), can be written in dimensionless cylindrical coordinates as

$$\frac{\partial F_1}{\partial T} R + \frac{\partial F_2}{\partial X} R + \frac{\partial (F_3 R)}{\partial R} = F_4 \tag{1}$$

where F_1, F_2, F_3, and F_4 are vector functions of the form

$$F_1 = \begin{vmatrix} G \\ GV \\ GU \\ E_1 \end{vmatrix}, F_2 = \begin{vmatrix} GU \\ GUV \\ GU^2 + P \\ (E_1 + P)U \end{vmatrix}, F_3 = \begin{vmatrix} GV \\ GV^2 + P \\ GUV \\ (E_1 + P)V \end{vmatrix}, F_4 = \begin{vmatrix} 0 \\ P \\ 0 \\ 0 \end{vmatrix}$$

where

$$E_1 = G[E + (U^2 + V^2)/2] \tag{2}$$

The variables in the above equations are conveniently non-dimensionalized in terms of r_0 (= a characteristic dimension of the original cloud), p_0 (= ambient pressure), ρ_0 (= ambient density), and $t_0 = r_0(\rho_0/p_0)^{1/2}$ (= the time it takes for an acoustic signal to propagate from the origin to r_0) The dimensionless independent variables are $X = x/r_0$, the coordinate along the axis of symmetry of the cloud, $R = r/r_0$, the coordinate representing the distance from the axis of symmetry, and $T = t/t_0$, the time The dimensionless dependent variables are the components of the flow velocity, $U = ut_0/r_0$, $V = vt_0/r_0$ in the direction of X and R, respectively, and the density, $G = \rho/\rho_0$, the pressure, $P = p/p_0$, and the internal energy, $E = e\rho_0/p_0$

The perfect gas equation of state is used in the two media in the form

$$P = (\gamma - 1)\, GE \tag{3}$$

A finite-difference method in accordance with the scheme proposed by Godunov et al [10] was used for the numerical solution of the problem formulated The fact that the basis for constructing the Godunov scheme uses conservation laws ensures that the approximate solution obtained with its aid will be close to the generalized solution of the equations of gas dynamics, even if these generalized solutions contain discontinuities (e g , shock waves, deflagrative waves and contact discontinuities) The work of these authors is of interest also because their numerical method may be utilized for calculations with a movable net This is convenient when one is carrying out gas dynamic calculations in regions where the boundaries are movable This difference scheme yields an approximation to the differential equations of first-order accuracy In developing the finite-difference scheme we adopted Shurshalov's [12] modification of the Godunov scheme, which presents the difference equations in a general form appropriate for calculations that are independent of the specific form of the grid for any mobile or immobile grid with four-cornered cells The numerical scheme treats the main shock wave and the moving surface which separates the burnt and unburnt gases as the boundaries of a moving grid network, ensuring the exact satisfaction of all the necessary conditions at these surfaces The treatment of the flame as a 'two-gamma'' working fluid model and all the relevant aspects of the boundary conditions and the computational scheme can be found in detail in Ref [13]

III. Acoustic solution for weak explosions

If the burning speed of the flame, M_{su}, is much smaller than 1, then the blast wave generated by deflagrative combustion can be described by acoustic theory Strehlow [6] extended the concept of the simple acoustic monopole theory to the case of arbitrary deflagrative explosions by treating the flame as a source of added volume The acoustic approach is useful to gain a qualitative understanding of the blast parameters when the numerical calculations of the 2-D and 3-D unsteady flows which result are complex and

expensive Thus, the numerical calculations of centrally ignited pancake-shaped clouds will be compared with the acoustic approximation in the weak deflagrative limit

Strehlow [6] shows that the acoustic pressure rise generated by deflagrative combustion of arbitrary wave shape in an infinite isentropic gas is given by

$$\bar{P} = \frac{p - p_0}{p_0} = \frac{\bar{Q}}{4\pi a_0^2 r} \frac{\mathrm{d}}{\mathrm{d}\tau} [S_u(\tau) A_f(\tau)] \tag{4}$$

where r is the distance, equal to or greater than r_f, τ is the retarded time, $t - r/a_0$, $S_u(t)$ is the effective normal burning velocity of the flame, $A_f(t)$ is the effective frontal area of the flame, and $\bar{Q}$ is the dimensionless heat addition, of which the relationship to the new volume produced per unit gas burned at constant pressure is

$$\frac{\bar{Q}}{\gamma_0} = \frac{\mathcal{V}_b - \mathcal{V}_u}{\mathcal{V}_u} \tag{5}$$

where γ_0 is the ratio of the specific heats

Figure 1 describes the flame processes occurring in the centrally ignited deflagrative combustion of the pancake-shaped cloud In the initial phase a spherical flame propagates until it reaches the outer edge of the cloud For a growing spherical ball

$$A_f = 4\pi r_f^2 \tag{6}$$

and

$$\frac{\mathrm{d}r_f}{\mathrm{d}t} = S_u \left(\frac{\mathcal{V}_b}{\mathcal{V}_u}\right) \tag{7}$$

From eqn (4), the acoustic pressure rise during the spherical flame propagation is

$$\bar{P} = \frac{\bar{Q}}{a_0^2 r} \left(\frac{\mathcal{V}_b}{\mathcal{V}_u}\right) \left[r_f^2(\tau) \frac{\mathrm{d}^2 r_f(\tau)}{\mathrm{d}\tau^2} + 2 r_f(\tau) \left(\frac{\mathrm{d}r_f(\tau)}{\mathrm{d}\pi} \right)^2 \right] \tag{8}$$

Deshaies and Leyer [14] obtained an identical expression from the integration of the conservation equations of mass and momentum for a spherical flow structure with a nonconstant velocity flame Conservation of mass yields the following expression for the final radius of the flame at the end of spherical combustion in terms of the original height of the cloud, $2H$,

$$r_s = \left(\frac{\mathcal{V}_b}{\mathcal{V}_u}\right)^{1/3} H \tag{9}$$

After the spherical flame breaks through the outer surface of the cloud, the flame propagates like an expanding cylindrical ring with an approximate height of $2r_s$ The effective area of the flame during this phase of flame

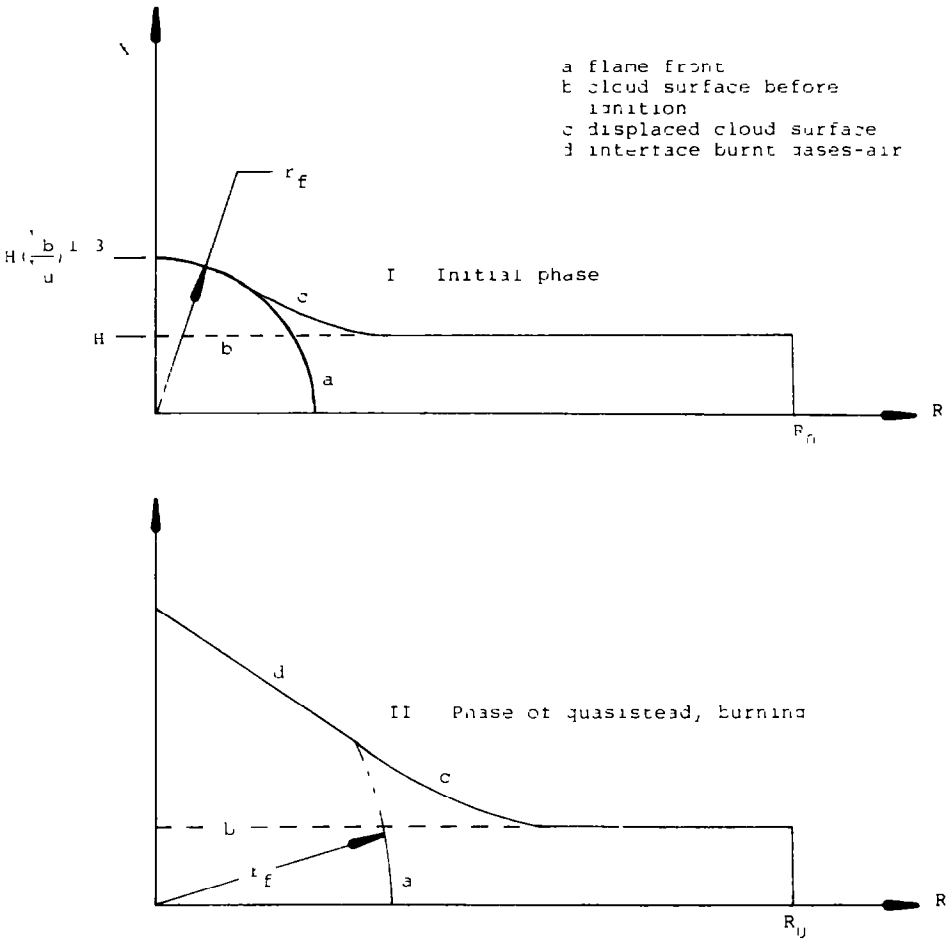

Fig 1 Schematic diagram of flame propagation in a pancake-shaped cloud

propagation is $4(\mathcal{V}_b/\mathcal{V}_u)^{1\,3}\pi\, r_f H$ and the acoustic pressure rise is given by

$$\bar{P} = \frac{\bar{Q}}{a_0^2}\left(\frac{\mathcal{V}_u}{\mathcal{V}_b}\right)^{2\,3}\left[\frac{d^2 r_f(\tau)}{d\tau^2}\, r_f(\tau) + \left(\frac{dr_f(\tau)}{d\tau}\right)^2\right]\left(\frac{H}{r}\right) \tag{10}$$

For constant velocity propagation, eqns (8) and (10) reduce to, respectively

$$\bar{P} = 2\bar{Q}\left(\frac{\mathcal{V}_b}{\mathcal{V}_u}\right) M_{su}^2\left(\frac{r_f(\tau)}{r}\right) \tag{11}$$

$$\bar{P} = \bar{Q}\left(\frac{\mathcal{V}_b}{\mathcal{V}_u}\right)^{2\,3} M_{su}^2\left(\frac{H}{r}\right) \tag{12}$$

From eqn (4), the expression for impulse is given by

$$I(t) = \int_0^t [p(t) - p_0]\,dt = \frac{p_0 \bar{Q}}{4\pi a_0^2 r} [S_u(\tau) A_f(\tau)]_0^t \tag{13}$$

Equation (13) shows that $I(t)$ is insensitive to the flame acceleration process or the change of flame surface with time The acoustic theory provides a solution in the region far from the flame front, and the solution breaks down in the region near the flame front where the flowfield is governed by the incompressible source flow [15] unless $M_{su} \ll 1$ No effort has been made to obtain the solution near the flame front as the potential flow theory requires a complete description of the interface of the burnt and unburnt gases with time Irrespective of the extreme simplifications introduced by using monopole theory, it is found to provide reasonable results, yielding the correct order of magnitude for peak overpressures in the weak deflagrative combustion limit of an explosion of an arbitrarily shaped source region

IV. Oblate-spheroid burst

As a specific example of a high-pressure burst we consider the blast wave generated by a pressurized oblate-spheroid burst of AR = (major axis/minor axis) = 5, with constant distribution of the gas-dynamic parameters over the source region corresponding to the constant volume combustion of methane—air mixture which is characterized by $P_b/P_u = 8\,934$, $G_b/G_u = 1$, $V_b = U_b = 0\,0$, $E_b = P_b/G_b(\gamma_2 - 1) = 44\,238$, $\gamma_1 = 1\,4$ and $\gamma_2 = 1\,202$

In Fig 2 the region originally occupied by the gas-cloud is shaded and the position and shape of the shock wave and contact surface at different times following the explosion are shown as solid and dashed lines Because of symmetry only one quadrant of a complete picture is shown After a large initial expansion there is a little movement of the edge of the source volume with time The shape of the shock wave is almost elliptical with a decaying ellipticity in time The shape of the lead wave approaches spherical as the lead shock gradually degenerates into an acoustic wave The experimental evidence of the blast waves generated by exploding wires [5] and condensed phase cylindrical wires [16] tends to confirm that the asymmetries present in the system smooth out as the blast wave progresses, and "far enough" from source, the waves become spherical

Figures 3—5 present the variation of pressure, density, and internal energy with distance at different times along the axis R Following the instant of burst, an expansion wave propagates into the source volume and a shock wave develops and propagates away from the source volume In the initial stages the strength of the rarefaction wave is so strong that it causes the source volume to expand almost at the sonic speed The peak overpressure in the system rapidly moves away from the source volume to the front of the lead wave that developed because of the expanding source volume The lead wave entraps a lot of mass as it propagates away from the source volume, raising the density of the inert medium behind the lead shock by a factor of

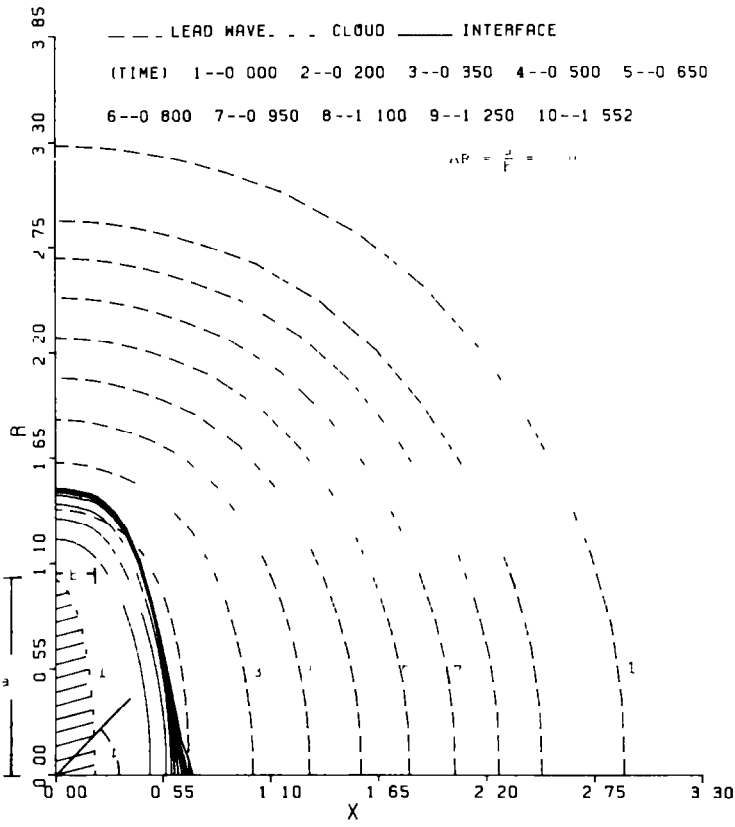

Fig 2 The positions of the interface and the lead shock at different times for the case of an oblate-spheroid burst

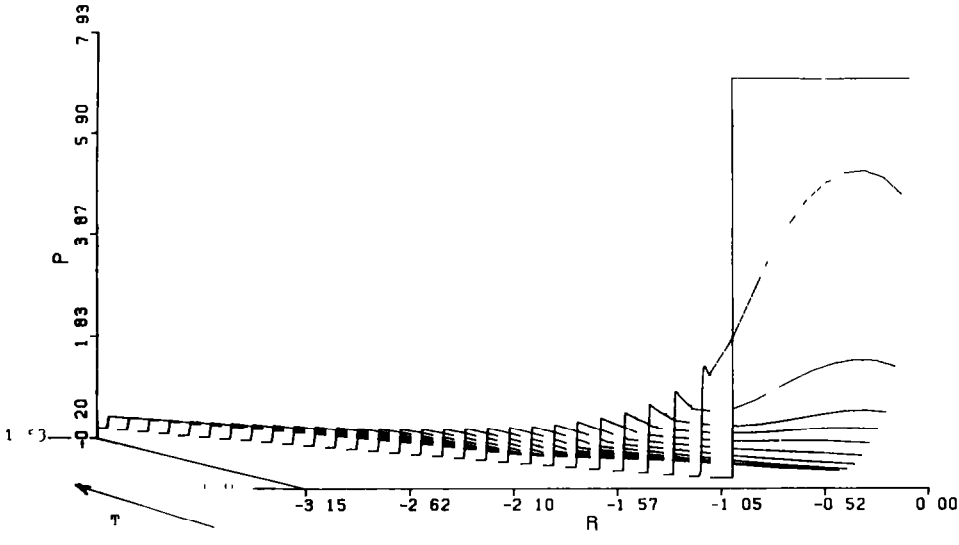

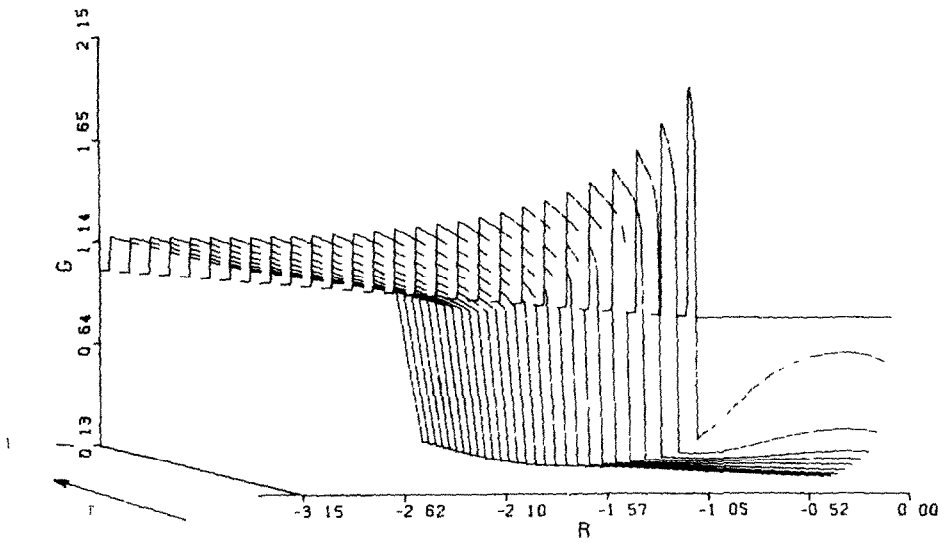

Fig 4 Density distribution versus distance and time generated by an oblate spheroid burst along the axis R

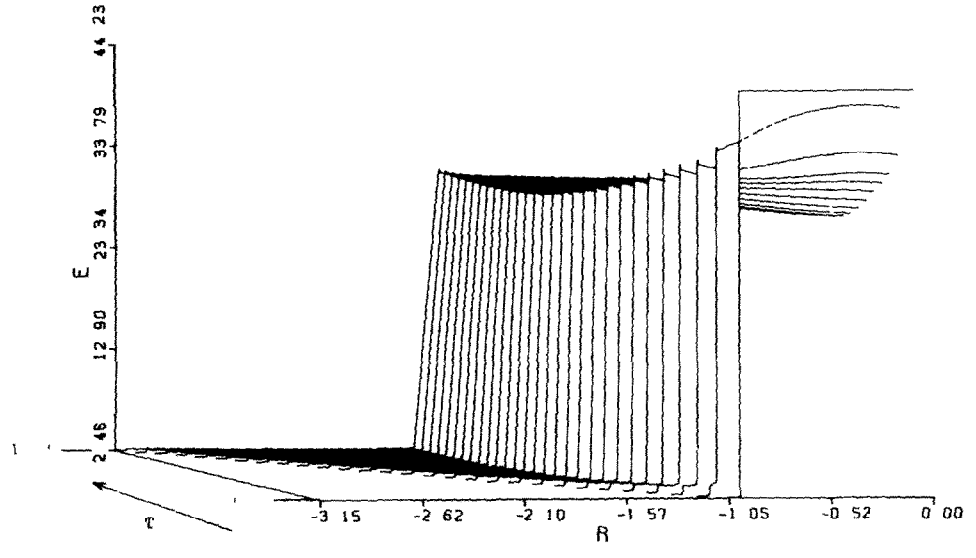

Fig 5 Internal energy distribution versus distance and time generated by an oblate spheroid burst along the axis R

Fig 3 Overpressure distribution versus distance and time generated by an oblate spheroid burst along the axis R

2 5 Another salient feature of the flowfield is that the magnitude of the pressure and density decrease continuously across the lead shock from $\phi = 0°$ to 90° The strength of the lead shock decreases monotonically as it propagates into the far field The expansion of the source volume continues until the density and internal energy of the burnt gases approach the values corresponding to those of a constant pressure deflagration

V Detonative combustion

Here we present the specific case of the detonative combustion of methane—air mixture, for a centrally ignited, pancake-shaped cloud of AR = (diameter/height) = 10 0, which is characterized by a Chapman—Jouguet detonation velocity of M_{su} = 5 1642, γ_1 = 1 4 and γ_2 = 1 2 In Fig 6 the region originally occupied by the cloud is shaded, and the position and shape of the lead shock and the interface of the burnt and unburnt gases at different times after the completion of the heat addition are shown as dashed and

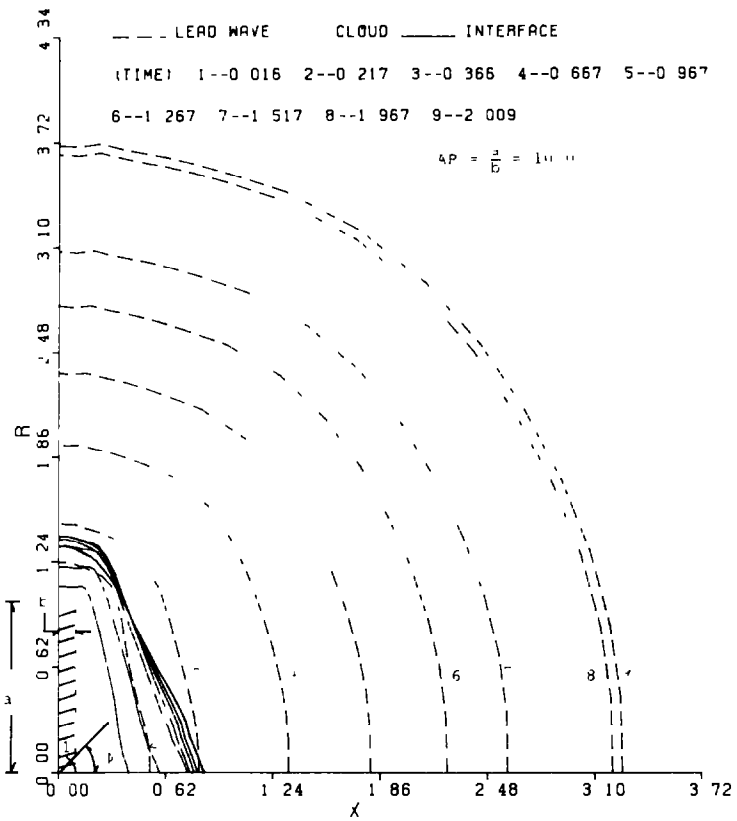

Fig 6 The positions of the interface and the lead shock at different times for the case of detonative combustion of a pancake shaped cloud with AR = 10

solid lines, respectively In the initial phase, a detonation front spreads spherically until it reaches the outer edge of the cloud at $T = 0\ 016$ as shown by curve 1 Following the initial spherical propagation the detonation front travels almost like an expanding cylindrical ring with X as the axis of symmetry Accompanying this phase of propagation, the detonation front will be followed by an expansion fan propagating from the compressible boundary into the combustion products while an oblique shock is induced in the inert compressible medium The wave interaction of the detonation products and the compressible medium, as shown in Fig 7, is greatly simplified but it helps to describe the salient features of the flowfield considered Figure 8 shows the results of the numerical calculations for the corresponding position and shape of the detonation front, the interface and the induced oblique shock front during this second phase of flame propagation at $T = 0\ 073$

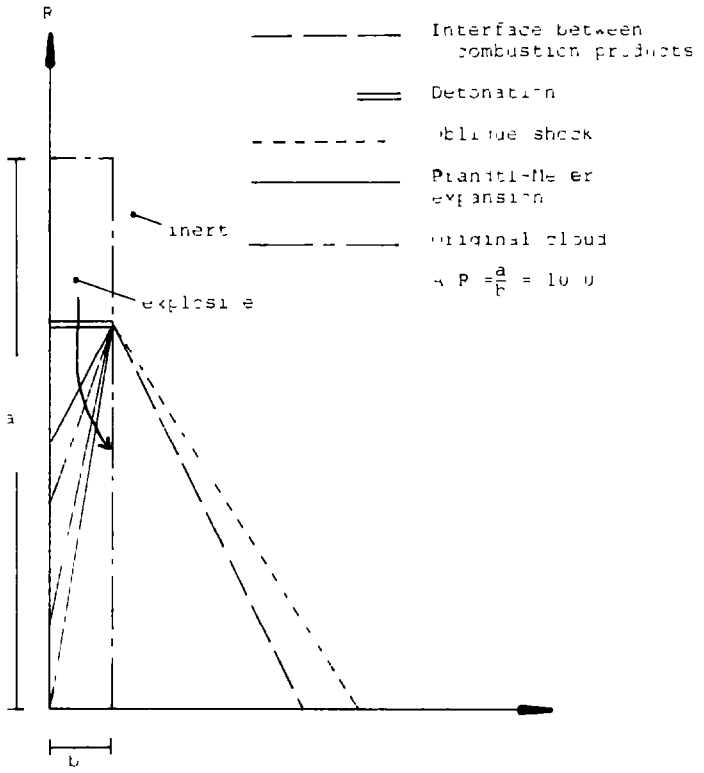

Fig 7 The wave interaction between the products of detonation and the inert compressible medium at the contact surface

There is no particle displacement in the flowfield ahead of the detonation front, and the induced shock and the conditions there remain at ambient during heat addition When heat addition is completed the induced shock separates from the source volume and propagates into the surroundings The

subsequent shapes of the lead shock and the interface at different times are given by curves 2 to 9 of Fig 6 As in the case of an oblate-spheroid burst, the source volume initially expands at the sonic speed and continues its expansion until the conditions of the flow inside the source volume attain values corresponding to constant pressure deflagration of the methane—air mixture

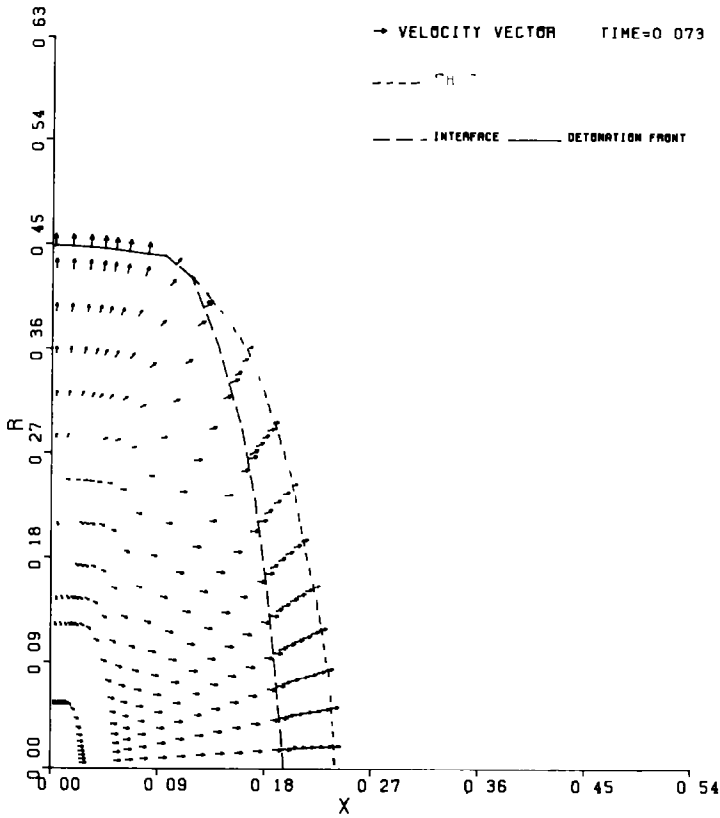

Fig 8 The velocity field at T = 0 073 generated by detonative combustion of a pancake shaped cloud with AR = 10

Figures 10—12 show the variation of pressure, density, and internal energy with distance at different times along the axis R During heat addition the overpressure at the detonation front corresponds to 15 72, which is the C—J value, and the pressure decreases monotonically towards the center as shown in Fig 10 Originating at the point of separation of the detonation front and the induced oblique shock, a strong rarefaction fan propagates into the combustion products, thereby restricting the high-pressure region to a

Fig 10 Overpressure versus distance and time generated by detonative combustion of a pancake-shaped cloud with AR = 10

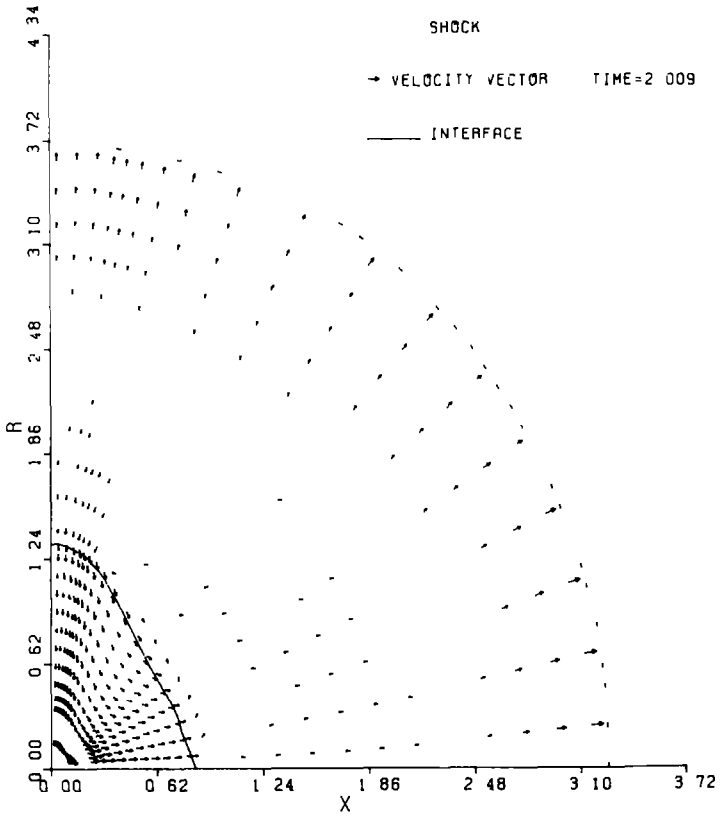

Fig 9 The velocity field at $T = 2\ 009$ generated by detonative combustion of a pancake shaped cloud with $AR = 10$

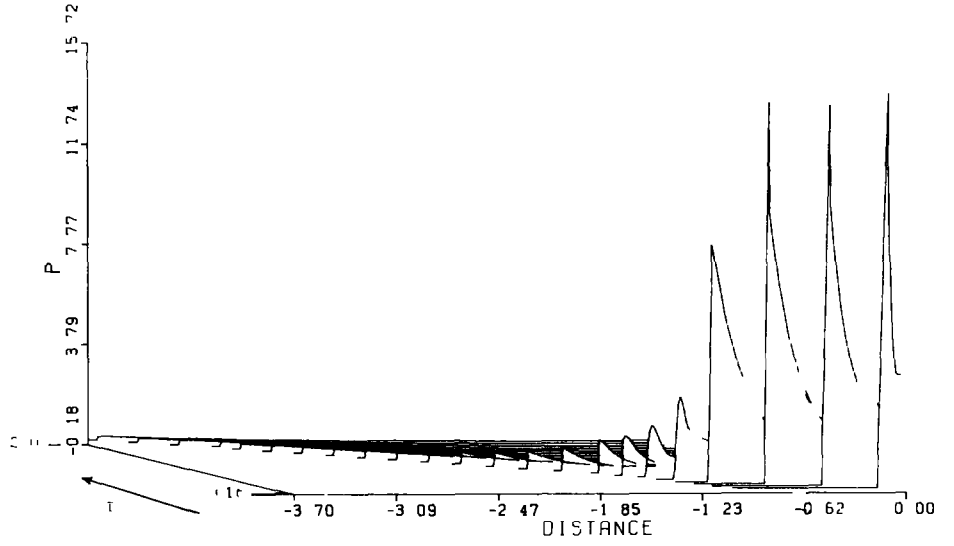

very narrow zone behind the detonation front during heat addition Subsequent to the completion of the heat addition the peak pressure in the system moves away from the detonation front to the lead shock The strength of the lead shock decreases monotonically as it propagates into the far field Figure 12 shows that the internal energy of the burnt gases go from a maximum of

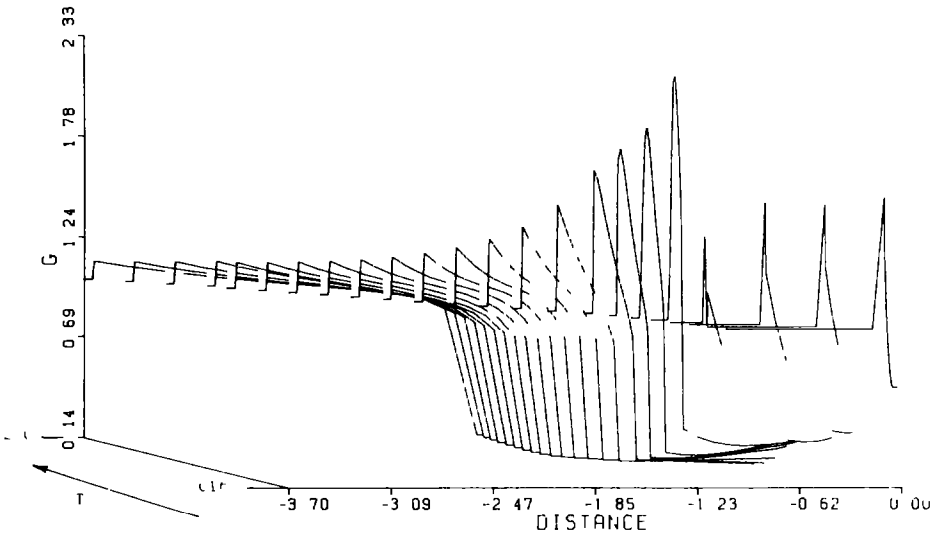

Fig 11 Density distribution versus distance and time generated by detonative combustion of a pancake-shaped cloud with $AR = 10$

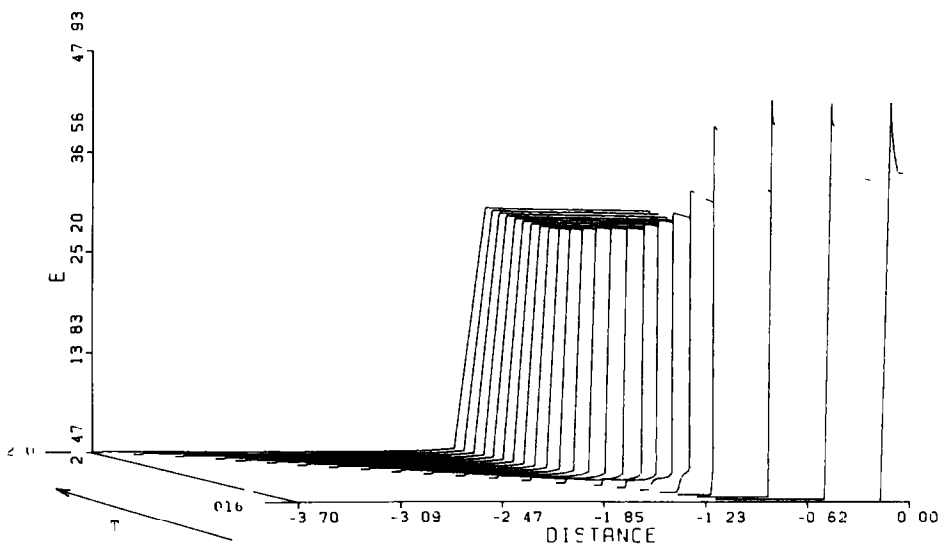

Fig 12 Internal energy distribution versus distance and time generated by detonative combustion of a pancake-shaped cloud with $AR = 10$

47 93 to 28, indicating that the detonative combustion is very effective in converting the internal energy to kinetic energy and thus more energy is made available to the surroundings Similar behavior is observed for the oblate-spheroid burst, but for deflagrative combustion there is little change in the internal energy of the burnt gases during and after energy addition Figure 11 shows trends in the behavior of the density which are similar to the case of the oblate-spheroid burst

Figures 8 and 9 show the velocity field at two different times At T = 0 073 the magnitude of the particle velocity varies from a maximum corresponding to the local speed of sound in the region immediately behind the detonation front to a minimum of zero at the stagnation region where the flowfield is changing its direction At T = 2 009 an expansion wave propagating towards the lead shock causes a change of the flow direction, which would otherwise be oriented towards the lead wave in the region outside of the source volume The flowfield in the source region near the origin appears to be similar to an ideal flow toward a "stagnation point" at a rigid boundary At this time there is very little movement of the edge of the source volume with time, as the magnitude of the particle velocities is very low

VI. Deflagrative combustion

Here we consider the specific example of centrally ignited deflagrative combustion of a pancake-shaped cloud with AR = 5 The thermodynamic properties of the hydrocarbon—air mixture are characterized by a volumetric expansion of 7 0 for a constant pressure deflagration, γ_1 = 1 3 and γ_2 = 1 2 The burning speed of the flame is assumed constant throughout the combustion process at M_{su} = 0 0428

Unlike detonative combustion the flowfield associated with deflagrative combustion is bounded by a lead shock front during flame propagation The particle velocity induced by deflagrative combustion, ahead of the flame front, continuously modifies the shape of the original cloud In the initial phase, when ignition occurs at the center of the cloud the flame spreads spherically until it reaches the outer surface of the cloud The corresponding shape and position of the flame and the displaced cloud are shown in curve 2 of Fig 13 In the next phase the flame propagates almost like an expanding cylindrical ring with X as the axis of symmetry until head addition is completed In curves 3—7 we show the positions of the flame, displaced cloud, and interface during and after the completion of heat addition The characteristic of this phase is the occurrence of pressure relief behind the flame front due to the upward expansion of the burnt gases In Fig 14 we show the pressure distribution along the axis R after the completion of the initial spherical deflagration In the case of deflagrative combustion the energy wave is propagating subsonically relative to both ambient conditions and conditions behind the energy wave There is a slight pressure rise along

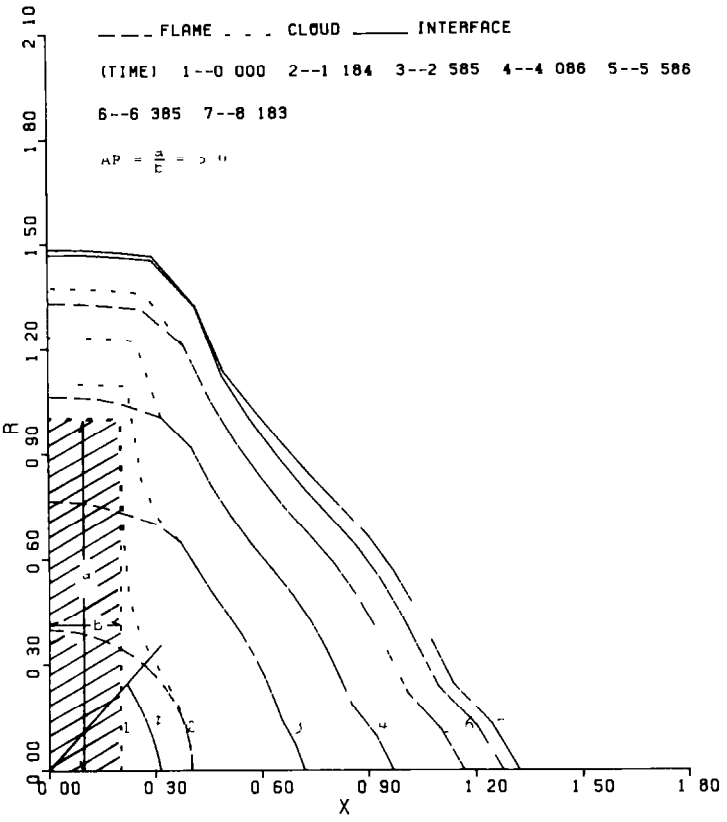

Fig 13 The positions of the flame, displaced cloud and interface at various times generated by deflagrative combustion of a pancake-shaped cloud with $AR = 5$ and $M_{su} = 0\ 0428$

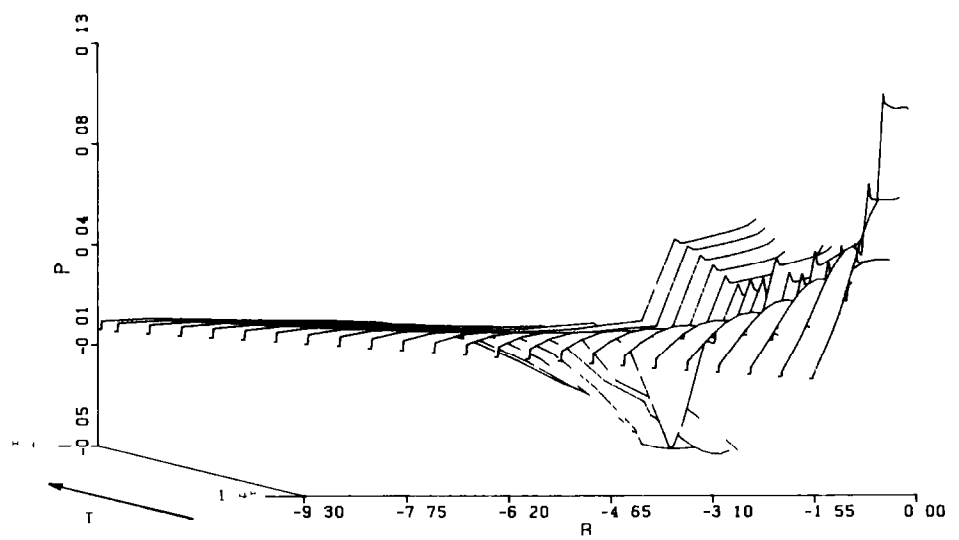

the shock Hugoniot followed by an isentropic compression to the beginning of the energy wave There is a large expansion and a slight pressure decrease through the energy addition with nearly equal density and pressure behind the energy wave during flame propagation The behavior of the blast field is similar to that of an acoustic field Recall from the discussion of the acoustic model that the rate of increase of the rate at which combustion products are formed plays an important role in determining the variations of the pressure distribution for low-velocity deflagrative combustion The initial high pressure in the system is characteristic of a spherical flame where the rate of the flame growth is very high and is proportional to r_f When the flame begins to propagate like an expanding cylindrical ring, the rate of the flame growth more or less remains constant and is proportional to the height of the cloud However, the acoustic pressure at the flame surface continues to decrease because the pressure not only depends on the flame growth but is inversely proportional to r_f The pressure in the system starts falling imme-

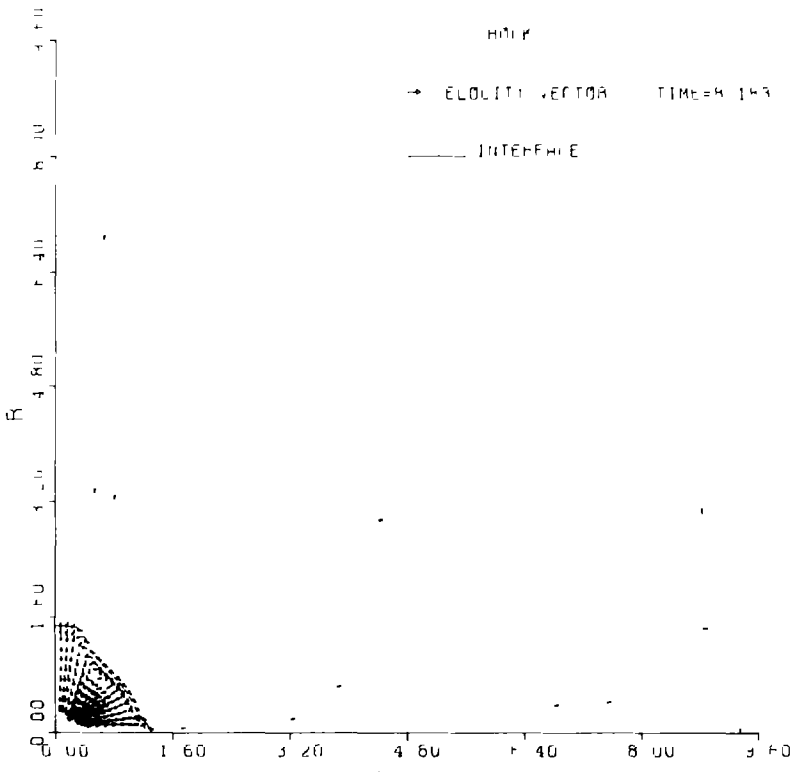

Fig 15 The velocity field at T = 8 8183 generated by deflagrative combustion of a pan cake-shaped cloud with AR = 5 and M_{su} = 0 0428

Fig 14 Overpressure distribution versus distance and time generated by deflagrative combustion of a pancake-shaped cloud with AR = 5 and M_{su} = 0 0428 along the axis R

diately after the initial spherical phase of combustion This effect can be clearly seen because a strong rarefaction wave originating at the edge of the source volume propagates towards the center, thereby decreasing the pressure within the source volume During the initial transition period after spherical flame propagation there is a rapid drop in pressure instead of a gradual drop predicted by the $1/r_f$ dependence of the acoustic model After heat addition stops, a rarefaction wave propagating from the edge of the source volume replaces most of the compression wave The duration of the negative phase is quite large The magnitude of the peak negative overpressure even exceeds the magnitude that the peak positive overpressure ever had There is considerable expansion of the source volume in the direction normal to the major dimension of the cloud traversed by the flame However, very little expansion of the source volume is observed after the completion of the energy addition Unlike spherical combustion, there is a large flow velocity imparted to the particles of the source volume during the flame propagation There is vortex formation within the source volume after the energy addition, as shown in Fig 15 The flow appears to be that generated by circular line vortices There is little variation in the values of the internal energy and density of the burnt gases during and after the completion of the heat addition It is also observed that the lead wave remains spherical at all times

VII. Blast parameters

The most important blast parameters, peak overpressure and positive phase impulse, which can be related to damage potential are nondimensionalized using Sachs's scaling relationship as presented by Baker et al [16]

$$\bar{P}_{\max} = \frac{p_{\max} - p_0}{p_0}$$

$$\bar{I}_+ = \frac{I_+ a_0}{E_t p_0^{2/3}}$$

where

$$I_+ = \int_{\substack{\text{positive} \\ \text{phase}}} [p(t) - p_0]\,dt$$

and E_t is the total energy that has been deposited in the source region Sachs has shown that $\bar{P}_{\max}$ and $\bar{I}_+$ are unique functions of a nondimensionalized distance in terms of an energy-scaled length parameter, $(E_t/P_0)^{1/3}$, for ideal sources such as condensed phase explosions

Peak overpressure, $\bar{P}_{\max}$, and dimensionless impulse for an oblate-spheroid burst as a function of the energy-scaled distance along $\phi = 0°$, $45°$ and $90°$ are shown in Figs 16 and 17, respectively For each case, the curves labeled

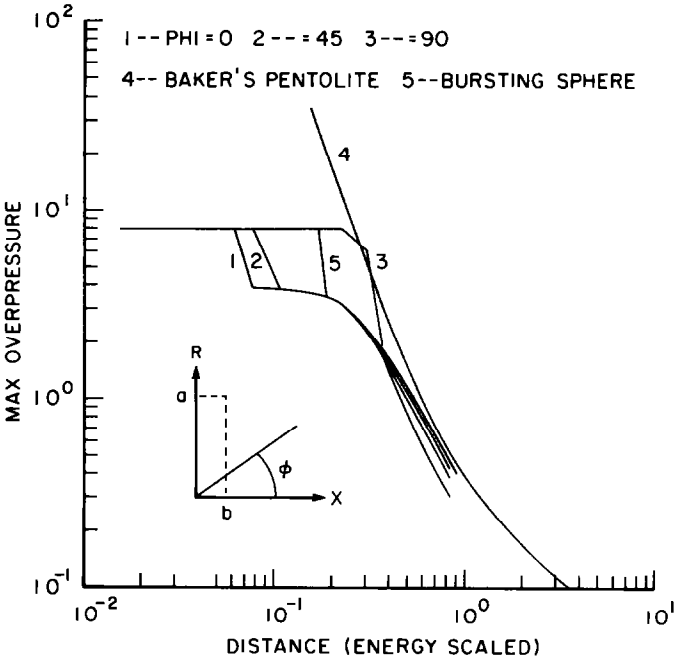

Fig 16 Peak overpressure versus energy-scaled distance generated by an oblate-spheroid burst

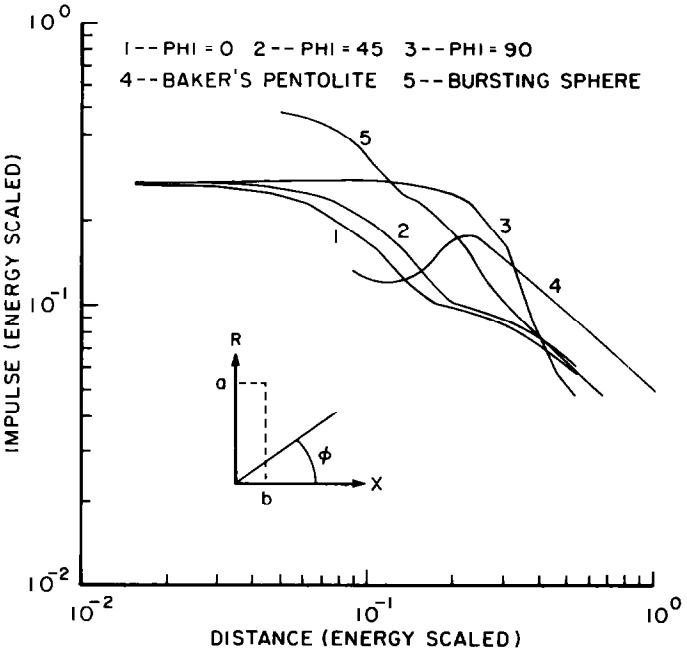

Fig 17 Energy-scaled impulse versus energy-scaled distance generated by an oblate spheroid burst

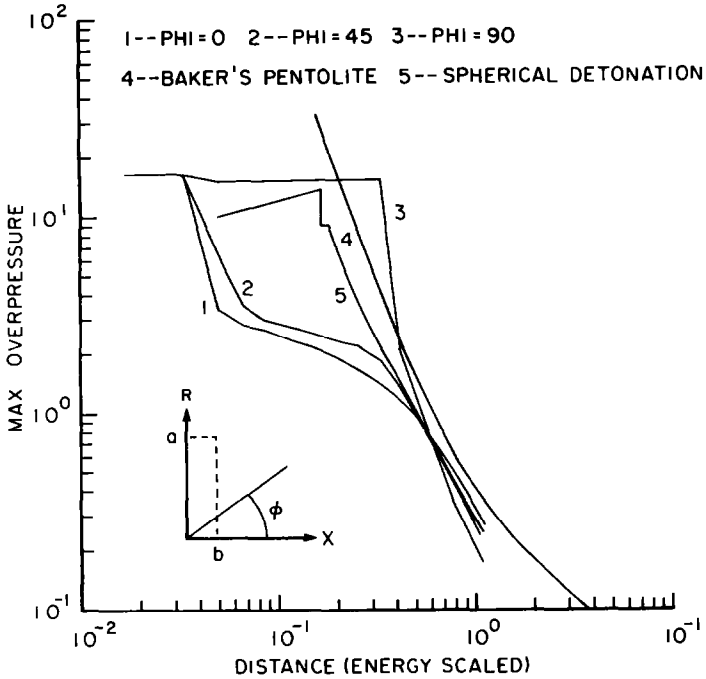

Fig 18 Peak overpressure versus energy-scaled distance generated by detonative combustion of a pancake-shaped cloud with $AR = 10$

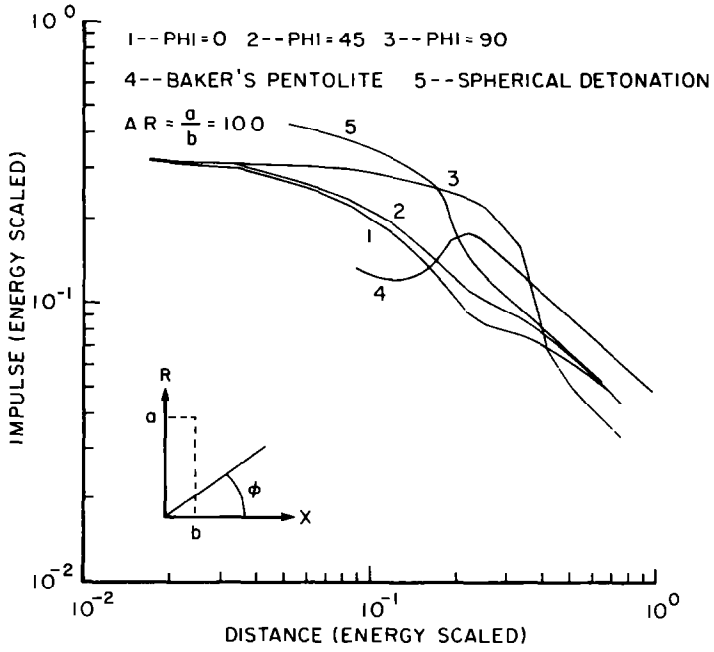

Fig 19 Energy-scaled impulse versus energy-scaled distance generated by detonative combustion of a pancake-shaped cloud with $AR = 10$

pentolite and bursting sphere are taken from Baker et al [16] for comparison In Fig 16 we note that the decay along the major axis, $\phi = 90°$, is much more rapid than the decay for the corresponding spherical burst or the decay along the minor axis, $\phi = 0°$ This is due to the large curvature of the shock wave near the major axis perpendicular to the (X, R) plane The shock decay approaches the spherical case along $\phi = 45°$ Impulse, which is a measure of the combined effect of the pressure rise over the ambient pressure at any location in the flowfield, decays at a much faster rate along the major axis when compared with the decay along the minor axis, indicating a high degree of directionality In the far field the decay along the minor axis coincides with the spherical case Both the impulse and peak overpressure curves lie below the pentolite curve in the far field as expected The peak overpressure and impulsive curves for a centrally ignited, pancake-shaped cloud of AR = 10 0 are shown in Figs 18 and 19, respectively The trend and behavior are similar to the oblate-spheroid burst

Figures 20—23 show peak overpressure as a function of the energy-scaled distance for different cases involving deflagrative combustion Figures 20 and 21 correspond to centrally ignited clouds of AR = 5 and 0 2, respectively

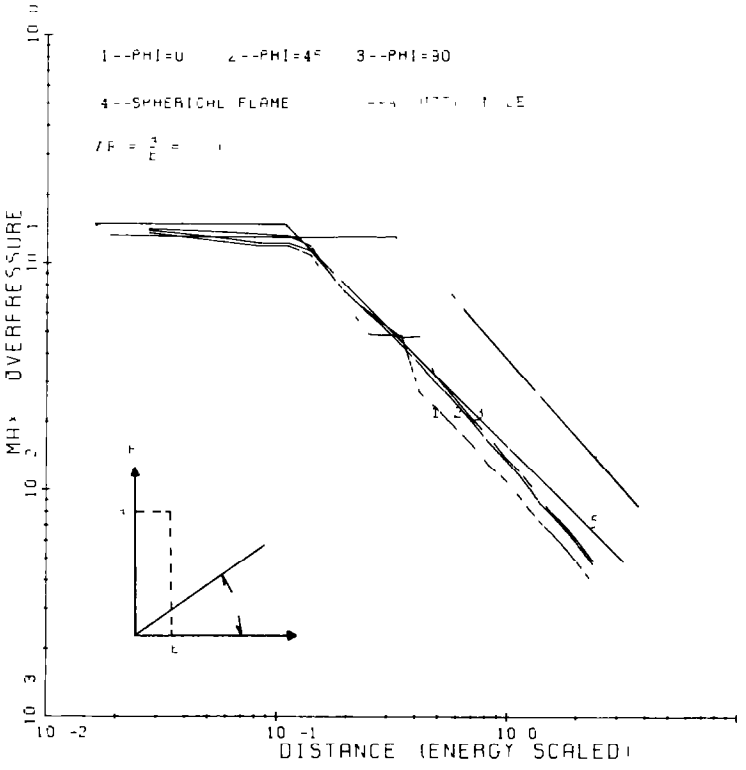

Fig 20 Peak overpressure versus energy-scaled distance generated by deflagrative combustion of a pancake-shaped cloud with AR = 5 and M_{su} = 0 0428

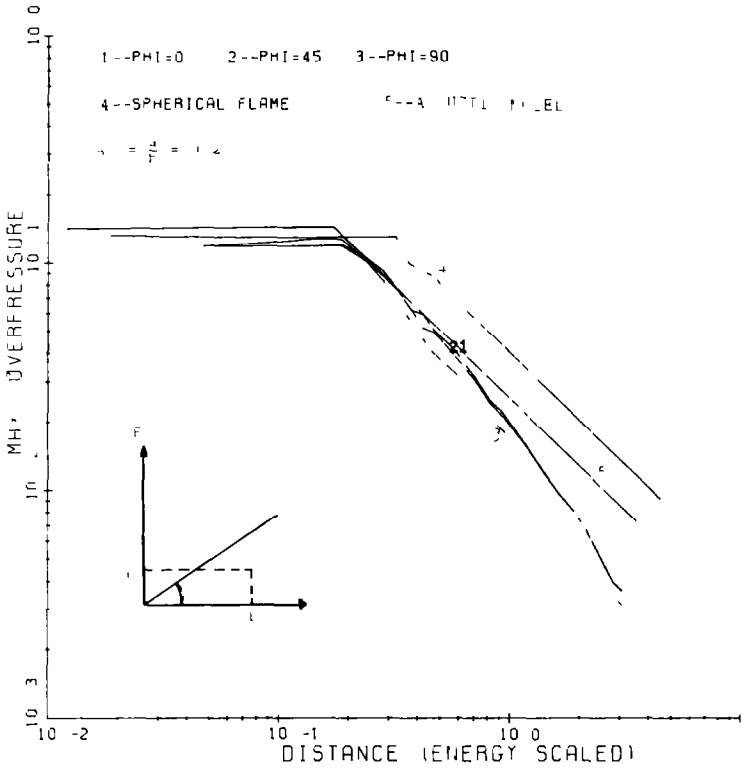

Fig 21 Peak overpressure versus energy-scaled distance generated by deflagrative combustion of a cigar-shaped cloud with AR = 0 2 and M_{su} = 0 0428

The burning speed in both cases is assumed constant at M_{su} = 0 0428 Figure 22 corresponds to the case of a pancake-shaped cloud with AR = 5 The burning speed of the initial spherical flame is assumed constant at M_{su} = 0 0428 followed by constant rate of acceleration, with a final burning speed attained by the flame at the end of heat addition corresponding to M_{su} = 0 1024 Figure 23 corresponds to the case of a pancake-shaped cloud of AR = 5 and constant burning speed of M_{su} = 0 1024 For each case, the corresponding curves for spherical deflagration of the same total energy and identical burning speeds are shown for comparison For weak deflagrative blasts the limiting solutions from acoustic theory are also plotted for comparison in Figs 20 and 21 In all these cases the initial high overpressures in the system are characteristic of the initial spherical flame After the flame reaches the edge of the cloud, further flame propagation through the cloud does not contribute very much to the peak overpressure curves, since the rate of flame area increase is very small after the completion of the initial spherical deflagration phase The pressure relief after burn through, associated with the deflagrative combustion of axisymmetric clouds, reduces blast

intensity in the far field Thus, the peak overpressure obtained using the spherical flame assumption becomes extremely conservative From Figs 20—23 it can be seen that the increased values of the peak overpressures resulting from the linear flame acceleration process do not exceed that produced by a flame which has sustained a constant burning speed of M_{su} = 0 1024, the highest burning speed at which the accelerating flame has propagated The simple acoustic monopole theory provides reasonable results for peak overpressure, yielding the correct order of magnitude for limiting cases of the deflagrative blast wave

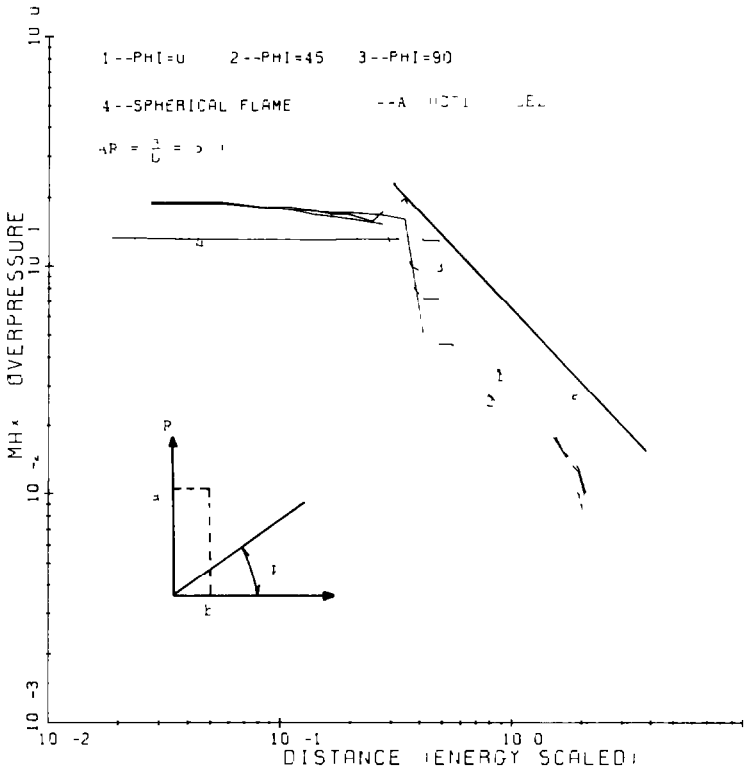

Fig 22 Peak overpressure versus energy-scaled distance generated by an accelerating flame propagation through a pancake-shaped cloud with AR = 5

VIII Conclusions

This study extends the numerical modeling of unconfined vapor cloud explosions to one more dimension to include the effects of the wave asymmetry by presenting a systematic study of the blast waves generated by a high-pressure oblate ellipsoid burst and axisymmetric deflagrative and detonative combustion processes By introducing appropriate modifications to

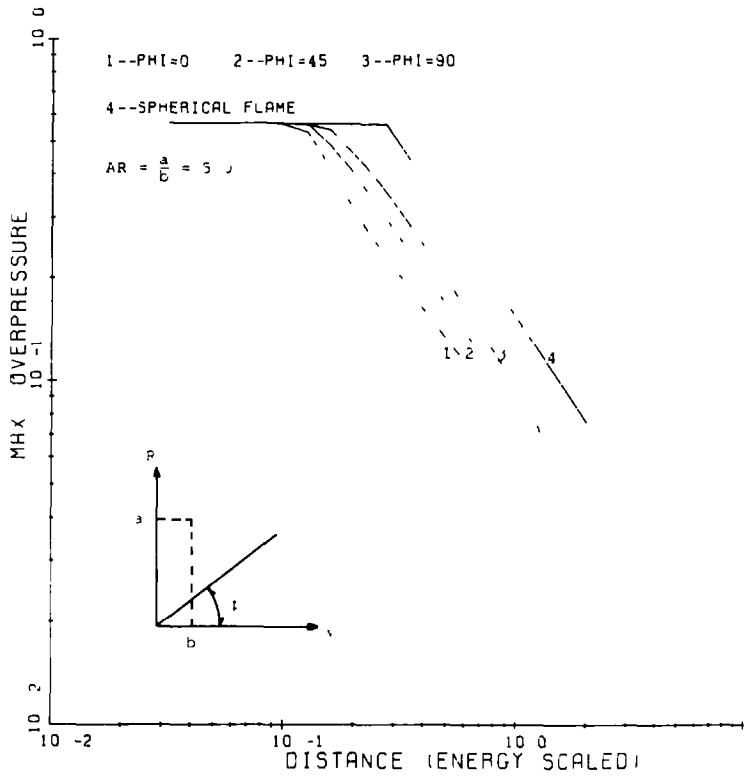

Fig 23 Peak overpressure versus energy-scaled distance generated by deflagrative combustion of a pancake-shaped cloud with $AR = 5$ and $M_{su} = 0\ 1024$

the scheme proposed by Godunov et al [10], the numerical integration of the 2-D nonsteady flows has been performed with the incorporation of a simple heat addition—working fluid model to adequately model a reactive Hugoniot For detonative and deflagrative combustion it is assumed that the flame velocity as function of time is known a priori The method of calculation permits detailed calculations of the blast structure during and after the propagation of a heat addition wave at any location in the flowfield For estimation of blast damage, plots of dimensionless peak overpressure and dimensionless impulse as a function of the energy-scaled distance are provided for various flame velocities and cloud geometries

The character of the blast waves associated with a high-pressure oblate ellipsoid burst or axisymmetric detonation are markedly different from the deflagrative combustion case The side relief associated with flame propagation through axisymmetric clouds severely restricts the intensity of the blast damage For deflagrative combustion of a centrally ignited, pancake-shaped cloud of $AR = 5$ a sustained effective burning velocity of $0\ 1024 \times 345 = 35$ m/s or 76 times the normal burning velocity of most hydrocarbons is needed

to produce an overpressure of 0 28 atm at the edge of the cloud This would be sufficient to cause minor structural damage and significant glass damage On the other hand, flames propagating through a centrally ignited spherical cloud require an effective normal burning velocity of only 21 m/s to produce an equivalent overpressure at the same location For an identical edge-ignited, pancake-shaped cloud acoustic theory predicts that the magnitude of the peak overpressures are less by an order of magnitude when compared to that of a centrally ignited spherical deflagration [6]

The results indicate that the deflagrative combustion of an extended cloud is very ineffective in producing damaging blast waves On the contrary, the pressure and impulse signatures of a high-pressure burst of an oblate ellipsoid and detonative combustion of axisymmetric clouds exhibit pronounced directional effects with very high overpressures near the source volume Hence, it appears likely that large flame accelerations and supersonic velocities close to C—J detonation velocities are needed if the combustion of an unconfined and extended cloud is to produce a damaging blast wave

List of symbols

a	velocity of sound
A	area
AR	aspect ratio
C—J	Chapman—Jouguet
e	specific internal energy
E, E_1	dimensionless specific internal energy
F_1, F_2, F_3, F_4	vector functions
G	dimensionless density
I	impulse
M	Mach number
p	pressure
P	dimensionless pressure
Q	dimensionless source energy density
r	radius or distance from the axis of symmetry
R	dimensionless distance or energy-scaled distance
t	time
T	dimensionless time
u	flow velocity in the direction of X-axis
U	dimensionless velocity in the direction of X-axis
v	flow velocity in the direction of R-axis
V	dimensionless velocity in the direction of R-axis
x	distance along X-axis
X	dimensionless distance along X-axis
γ	specific heat ratio
ϕ	angle in degrees with the positive direction of X-axis
ρ	density

τ	retarded time, $t - r/a$
$\mathcal{V}$	volume of gases

Superscripts

—	dimensionless quantity

Subscripts

+	positive phase
0	ambient condition
1	state 1 (ahead of the steady wave)
2	state 2 (behind the steady wave)
b	burnt gases
f	flame
max	maximum
s	end of spherical combustion
su	flame velocity relative to flow ahead
t	total
u	unburnt gages

References

1 G I Taylor, Proc Roy Soc A186 (1946) 273
2 A L Kuhl, M M Kamel and A K Oppenheim, 14th Symposium (International) on Combustion, The Combustion Institute, 1973, p 1201
3 R A Strehlow, 14th Symposium (International) on Combustion, The Combustion Institute, 1973, p 1189
4 T R Auton and J H Pickles, Central Electricity Research Laboratories, Laboratory Note No RD/L/N 210/78, 1978
5 K Chiu, J Lee and R Knystautas, J Fluid Mech , 82 (1977) 193
6 R A Strehlow, 13th AIChE Loss Prevention Symposium, Philadelphia PA, 1981
7 J H Pickles and S H Bittleston, Combust Flame, 51 (1983) 45
8 M Sickel and J C Foster, Acta Astronautica, 6 (1979) 243
9 F A Williams, J Fluid Mech , 127 (1983) 429
10 S K Godunov, A V Zabrodin and G P Propokov, J U S S R Comp Math Math Phys , 1 (1962) 1187
11 R A Strehlow, R T Luckritz, A A Adamczyk and S A Shimpi, Combust Flame, 35 (1979) 297
12 L V Shurshalov, J U S S R Comp Math Math Phys , 13 (1973) 186
13 M S Raju, The blast waves from unconfined axisymmetric vapor cloud explosions, Ph D Thesis, Dept of Aeronautical Engineering, University of Illinois at Urbana-Champaign, 1982
14 P Deshaies and J C Leyer, Combust Flame, 40 (1981) 141
15 L D Landau and Lifshitz, Fluid Mechanics, Vol 6 of Course of Theoretical Physics, Pergamon Press, U S A , 1959
16 W E Baker, P A Cox, P S Westine, J J Kulrsz and R A Strehlow, Explosions Hazards and Evaluation, Elsevier, Amsterdam, 1983